This manuscript has been submitted for publication in JOURNAL OF ATMOSPHERIC AND OCEANIC TECHNOLOGY in Aug 2023. Please note that, despite having undergone peer-review, the manuscript has yet to be formally accepted for publication. Subsequent versions of this manuscript may have slightly different content. If accepted, the final version of this manuscript will be available via the 'Peer-reviewed Publication DOI' link on the right-hand side of this webpage. Please feel free to contact any of the authors; we welcome feedback

Reconstructing Global Ocean Color Data at High Temporal Resolution Using an Improved DINEOF Algorithm

Haipeng Zhao,[a,b] Atsushi Matsuoka,[c] Manfredi Manizza,[d] Amos Winter[a]

[a] *Department of Earth and Environmental Systems, Indiana State University, Terre Haute, IN, USA.*

[b] *Division of Earth and Climate Sciences, Nicholas School of the Environment, Duke University, Durham, NC, USA.*

[c] *Institute for the Study of Earth, Oceans, and Space, University of New Hampshire, Durham, NH, USA.*

[d] *Geosciences Research Division, Scripps Institution of Oceanography, University of California, San Diego, La Jolla, CA, USA.*

Corresponding author: Haipeng Zhao (h.zhao@duke.edu)

ABSTRACT

Global studies on phytoplankton phenology remain challenging primarily because of sparse observations. The Data Interpolation Empirical Orthogonal Function (DINEOF) algorithm has been used successfully to reconstruct datasets of geophysical and biological variables such as sea surface temperature (SST) and Chlorophyll *a* (Chl *a*). We propose an improved version of DINEOF, DINEOF+, based on a comprehensive validation that show DINEOF+ is an appropriate method for studying chlorophyll *a* (Chl *a*) concentrations in the ocean. Error analysis reveals that 75 percent of missing data (PMD) is a reasonable threshold for applying DINEOF+ to reconstruct incomplete datasets. DINEOF+ improves accuracy over the original DINEOF by integrating connectivity filter that further reduces the errors caused by missing data. We successfully apply DINEOF+ to the OC-CCI global daily Chl *a* dataset. We find that the recovery rate varies across ocean basins and years. In oligotrophic waters, the daily data coverage increased by 40–50% during the period from 2003 to 2020. Using DINEOF+ allows us to obtain a significantly higher temporal resolution of global Chl *a* data, which will improve understanding of marine phytoplankton dynamics in response to changing environments.

SIGNIFICANCE STATEMENT

Global studies on marine ecosystems are hindered by sparse observations. We propose an upgraded version of the Data Interpolation Empirical Orthogonal Function algorithm, DINEOF+, to reconstruct global ocean color data. A comprehensive validation proves that DINEOF+ is an appropriate method for recovering missing data from satellite-derived chlorophyll *a* datasets. DINEOF+ could also be applied to other biogeochemical variables. Using DINEOF+ in such application will greatly improve understanding of biogeochemical processes in the oceans.

1. Introduction

Over the last two decades, observational and modeling studies have shown that ocean warming is driving changes in phytoplankton production and distribution (Behrenfeld et al. 2006; Benedetti et al. 2021; Gobler et al. 2017). Increased frequency of extreme events and variations in nutrient supply as a result of both changing circulation and stratification are likely to reorganize the dynamics of phytoplankton communities, leading to far-reaching impacts on local ecosystems and human society (Huntington et al. 2020; Smith et al. 2021).

Nevertheless, the task of establishing concrete connections between environmental variables and phytoplankton response has been formidable (Behrenfeld and Boss 2014).

The use of ocean color data, combined with *in situ* measurements and model outputs, has emerged as one of the best ways to detect regional trends in phytoplankton changes and reveal a possible link with environmental forcing factors. The ocean color is referred to spectrally resolved water-leaving radiance and inferred biogeochemical variables such as Chlorophyll *a* (Chl *a*) concentration. Uncertainties in the retrieved ocean color data are associated with atmospheric correction and in-water algorithms, and instrument performance. Many studies have employed satellite-derived Chl *a* to assess a long-term trend associated with environmental factors such as temperature and mixed layer depth that determine phytoplankton phenology and primary production in high-latitude oceans (Kahru et al. 2011; Lewis et al. 2020; Zhao et al. 2022). Despite these efforts, data gaps in ocean color products stand out as a significant factor for time-series analysis. Contaminated pixels caused by sun-glint, sea ice, as well as persistent cloud cover significantly reduce the number of available pixels that can be detected by satellite-based sensors (Blondeau-Patissier et al. 2014).

To fill the gaps caused by these issues, composite data is often generated using all available values for a given period (e.g. 8-day mean) or by re-gridding data into a coarser grid. Both strategies can help increase data coverage, however, it is still insufficient to accurately determine the phenological metrics (Cole et al. 2012). The same problem remains when multi-sensor merged products are employed, as the daily data coverage reaches only up to 25% of the world ocean (Maritorena et al. 2010). The imperative search for broader coverage and improved detection of both temporal and spatial variations of phytoplankton biomass motivates further research into effective methods for interpolating missing data.

Data Interpolation Empirical Orthogonal Functions (DINEOF) is a classic technique to reconstruct incomplete datasets on geophysical variables (Beckers and Rixen 2003). It is a variant of learning algorithms that use matrix factorization to address missing data problems. Thus, it has generally superior performance and accuracy over linear interpolation (Ghahramani and Jordan 1993). Additionally, DINEOF is initially parameter-free, fast convergent, and independent of a priori information, which permits its wide application to geophysical datasets. Two most successful examples include satellite-derived data on sea surface temperature (SST) and sea surface salinity (SSS) (Alvera-Azcárate et al. 2005; Alvera-Azcárate et al. 2007; Alvera-Azcárate et al. 2016). In contrast, its applicability to

biogeochemical variables (such as Chl *a*) is questionable given their high spatiotemporal heterogeneity (i.e. a greater variance occurs in a small scale) in the upper ocean (Mahadevan 2005). Regardless, recent studies have applied DINEOF to recover missing data in Chl *a* product. The impacts of missing data on reconstructed values are often ignored and there is also a lack of sufficient validation (Hilborn and Costa 2018; Liu and Wang 2018, 2019; Marchese et al. 2022).

This study proposes an improved DINEOF (hereafter referred to as DINEOF+) that is applicable to an ocean color product based on a comprehensive basin-wide evaluation across global oceans. We aim to provide conditions under which DINEOF+ can be applied to recover missing ocean color data with statistical confidence by evaluating the impacts of missing data on a global scale. Furthermore, as a proof of concept, we attempt to apply DINEOF+ to reconstruct global satellite Chl *a* products to obtain high temporal resolution ocean color dataset for advancing our knowledge about phytoplankton dynamics including its phenology across the global ocean.

The paper is organized as follows: Section 2 describes the main steps of DINEOF+ and provides additional information on its properties. The results of the evaluation are presented in section 3, where we analyze the impacts of missing data. Section 4 presents the reconstructed datasets on global daily Chl *a* after applying the method. Section 5 presents the validation via comparison to *in situ* data. In section 6, we discuss the obtained results and summarize the implications of our research study.

2. Method

a. DINEOF algorithm

Denote the data matrix $\mathbf{A}$ whose entry $(i, j) \in [m] \times [n]$ corresponds to the observation of the variable $f(r_i, t_j)$ at location r_i and moment t_j:

$$\mathbf{A}_{ij} = f(r_i, t_j) \tag{1}$$

The empirical orthogonal functions (EOFs) can be calculated based on singular vector decomposition (SVD) by solving:

$$\mathbf{A}\mathbf{A}^{\mathrm{T}}\mathbf{u} = \sigma^2\mathbf{u} \tag{2}$$

$$\mathbf{A}^{\mathrm{T}}\mathbf{A}\mathbf{v} = \sigma^2\mathbf{v} \tag{3}$$

where u and v are referred to as spatial and temporal EOFs, respectively. σ represents singular value.

Thus, the initial matrix can be decomposed as:

$$\mathbf{A} = \sum_{i=1}^{r} \sigma_i \mathbf{u}_i \mathbf{v}_i \tag{4}$$

where $r = rank(\mathbf{A}) \leq min\,(m, n)$.

In situations where $\mathbf{A}$ is incomplete, the unknown entries $\mathbf{A}_{ij}^{u}$ are estimated by using the truncated series of the first *k* EOFs, $\sum_{i=1}^{k} \sigma_i \boldsymbol{u}_i \boldsymbol{v}_i$. Then the EOFs are recalculated to update the previous estimations of the missing data. The main steps of DINEOF algorithm are summarized in Table 1.

Table 1. Summary of the main steps of DINEOF.

Algorithm DINEOF

1. Set the initial value $\mathbf{X}_{ij}^{o}$ for unknown entries $\mathbf{A}_{ij}^{u}$
2. **For** each number of EOFs *k* **do**
3. **while** in the t^{th} iteration of using *k* number of EOFs **do**
4. Fill $\mathbf{A}$ by replacing unknown entries $\mathbf{A}_{ij}$ with $\mathbf{X}_{ij}^{t-1}$, denote the filled matrix as $\mathbf{A}^{t}$
5. Compute the top *k* singular vectors $\mathbf{u}_i$, $\mathbf{v}_i$, and singular values σ_i of $\mathbf{A}^{t}$
6. $\mathbf{X}_{ij}^{t} = \sum_{i=1}^{k} \sigma_i \boldsymbol{u}_i \boldsymbol{v}_i$
7. **end while**
8. **end for**

More detailed procedures have been described in previous studies (Alvera-Azcárate et al. 2005; Beckers and Rixen 2003; Liu and Wang 2019; Zhao 2023). However, we realize that there is a lack of explanation in terms of several important properties (e.g. convergence). Here, we provide some theoretical foundation for this algorithm:

(1) Convergence

The principle of DINEOF is equivalent to maximum likelihood estimation (MLE) for solving a latent-variable model. The iteration of SVD with missing values can be expressed by the Expectation-Maximization (EM) procedure, which ensures convergence (Sheng et al. 2005) assuming that the spatiotemporal data matrix is represented by a *k*-rank linear model plus noise with a Gaussian distribution (see Appendix B).

(2) Initial values X_{ij}^{o}

DINEOF relies on pre-imputation to fill in missing data for implementing SVD. To have an unbiased estimation, imputation by the average of the matrix provides better performance than that by zeros and column-based average (Kurucz et al. 2007). In practice, the average is subtracted during the entire process, so the missing data is initially assigned with zeros. We notice that the use of a log-transformed matrix will improve the accuracy of recovered Chl *a* data.

(3) Optimal number of EOF

While *k* is fixed in each iteration, most algorithms choose to increase *k* as the iteration proceeds until a local optimal result is achieved or it reaches a maximum number. As an unsupervised process, the optimal number of EOF may vary each time due to the random selection of samplings for cross-validation. It should be noted that the process tends to be overfitted as the number of EOFs increases, resulting in reduced accuracy of recovered elements (Yang et al. 2023).

b. Connectivity filter

The performance of DINEOF is affected by the presence of missing data in the matrix. Ocean color data is often characterized by a large number of missing data that are unevenly distributed along both spatial and temporal dimensions. This results in unpredictable errors in the reconstructed matrix. To improve the accuracy of DINEOF reconstruction, this study proposes an integration of the original DINEOF and connectivity filter, which is explained below:

Based on the principle that DINEOF utilizes information along two dimensions (i.e. time and space in satellite data; see Figure 1a) to reconstruct missing values, two conditions are examined to identify those pixels that are unrecoverable: (1) spatial connectivity and (2) temporal connectivity. If there is at least one observed value neighboring the pixel along a spatial dimension, the pixel is defined as spatially connected. Similarly, the pixel is defined

as temporally connected when there is at least one neighboring pixel observed along the temporal dimension. The pixels that are neither spatially nor temporally connected are removed from the final reconstructed matrix. In our study, the spatial connectivity is set as a neighboring structure of size 8 (Figure 1b), and the temporal connectivity is set as a neighboring structure of size 6 (Figure 1c). Hereafter DINEOF+ is referred to as the merging of the connectivity filter with the original DINEOF.

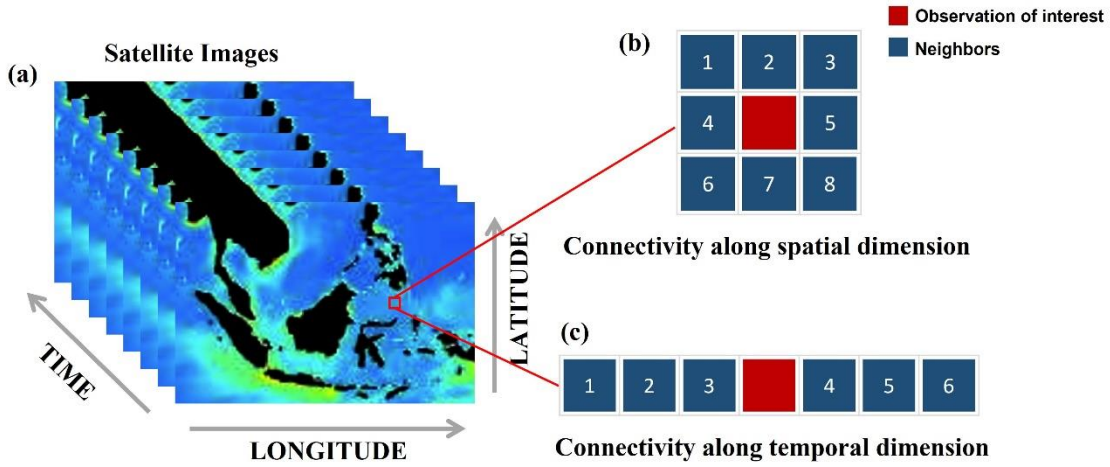

Fig. 1. Illustration of connectivity filter method. (a) Data structure of time-series satellite images; (b) 8-neighbor structure of connectivity along spatial dimension; (c) 6-neighbor structure of connectivity along temporal dimension.

3. Evaluation of impacts of missing data

a. Test data

The global daily chlorophyll concentration in 2019 at 0.25° × 0.25° is obtained from Copernicus Marine Services (https://marine.copernicus.eu/). It is derived from PISCES biogeochemical model on the NEMO (version 3.6) platform (Aumont et al. 2015). To evaluate impacts of the variance of Chl *a* magnitude on the performance of DINEOF+, the datasets are selected from nine testing areas each with different trophic levels defined by their range of Chl *a* (Antoine et al. 1996). This is comprised of three oligotrophic regions (Chl ≤ 0.1 mg m^{-3}), three mesotrophic regions (0.1 < Chl ≤ 1 mg m^{-3}), and three eutrophic regions (Chl > 1 mg m^{-3}) (Figure 2, Table 2). These datasets are used in three ways: 1) Find the threshold of missing data for applying DINEOF, 2) Determine the impact of the distribution

of missing data on the performance of DINEOF, and 3) Evaluate the performance of DINEOF after integrating connectivity filter (DINEOF+).

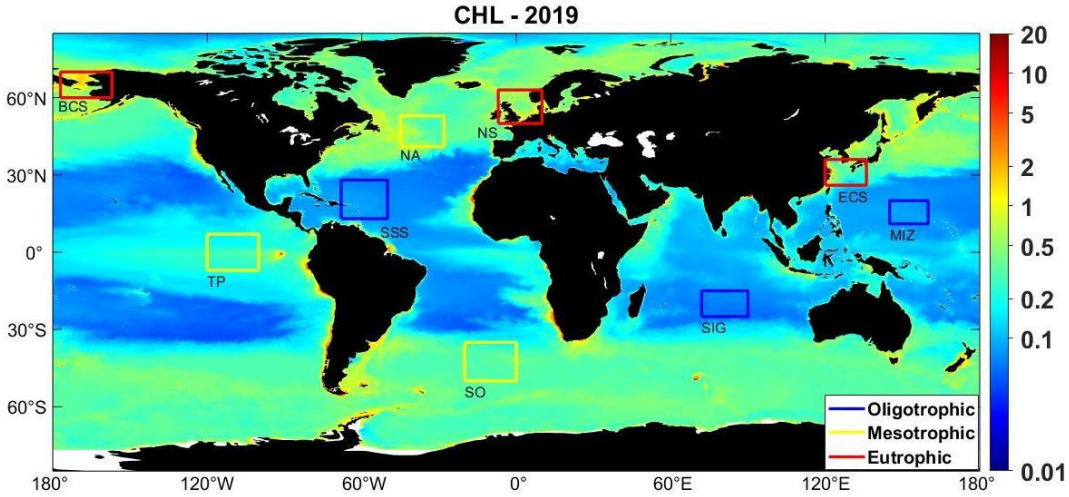

Fig. 2. Global map of annual Chl *a* concentration from NEMO-PISCES model in 2019. Testing areas include 3 oligotrophic regions (blue boxes), 3 mesotrophic regions (yellow boxes orange), and 3 eutrophic regions (red boxes).

Table 2. Statistics of Chl *a* magnitude in testing areas from the global daily dataset in 2019. Notes: Mean is the average value; STD is the standard deviation, *n* is row number along latitude, *m* is column number along longitude, *t* is number of days for one year.

Regions	**Size (*n**m*t)**	**Mean (mg m^{-3})**	**STD (mg m^{-3})**
Oligotrophic			
South Sargasso Sea (SSS)	71 * 59 * 365	0.0799	0.0111
Southern Indian Gyre (SIG)	71 * 39 * 365	0.0687	0.0115
Mariana Island Zone (MIZ)	59 * 35 * 365	0.0853	0.0117
Mesotrophic			
North Atlantic (NA)	67 * 47 * 365	0.4093	0.2977
Southern Ocean (SO)	79 * 59 * 365	0.3052	0.0993
Tropical Pacific (TP)	79 * 55 * 365	0.2288	0.0628
Eutrophic			
East China Sea (ECS)	63 * 39 * 365	0.4931	0.9193
Bering-Chukchi Sea (BCS)	79 * 39 * 365	0.8947	0.9561

North Sea (NS)	67 * 51 * 365	0.6844	0.6017

b. Threshold of the percentage of missing data

We first prepare the data matrix, $\mathbf{A}^o$, by randomly removing 1% of the pixels from the original data and then generate a reconstructed dataset. We repeat this procedure by removing an additional 1% of the original pixels through several iterations until 95% of the data is removed to assess the impact of missing data on reconstructed results derived by DINEOF+. Selected error metrics for algorithm evaluation include bias, median absolute error (MAE) (Eq. (1) and Eq. (2)), root mean square error (RMSE), regression slope, and r^2. All data values are log-transformed prior to the calculation of the error metrics.

$$\text{bias} = 10^{median\left(log_{10}(\mathbf{M}_i) - log_{10}(\mathbf{O}_i)\right)} \tag{5}$$

$$\text{MAE} = 10^{median\left(|log_{10}(\mathbf{M}_i) - log_{10}(\mathbf{O}_i)|\right)} \tag{6}$$

Where $\mathbf{O}_i$ is the model value as reference solution, $\mathbf{M}_i$ is the estimated value, $i = 1, 2, \ldots n$ and n is the extent of missing data.

Here, we select MAE as the representative error metric. Figure 3 shows the errors consistently increase with the percentage of missing data (PMD) in all testing areas. In oligotrophic regions, the magnitude of errors ranges from 1.005 to 1.04 when the PMD increases from 1–95%. In the mesotrophic and eutrophic regions, the ranges are 1.01–1.10% and 1.04–1.24% respectively. We found the two-term exponential model fits the trends of MAE with r^2 above 0.99 for all testing areas. It predicts that the PMD is 76–84%, when MAE increases by 100%.

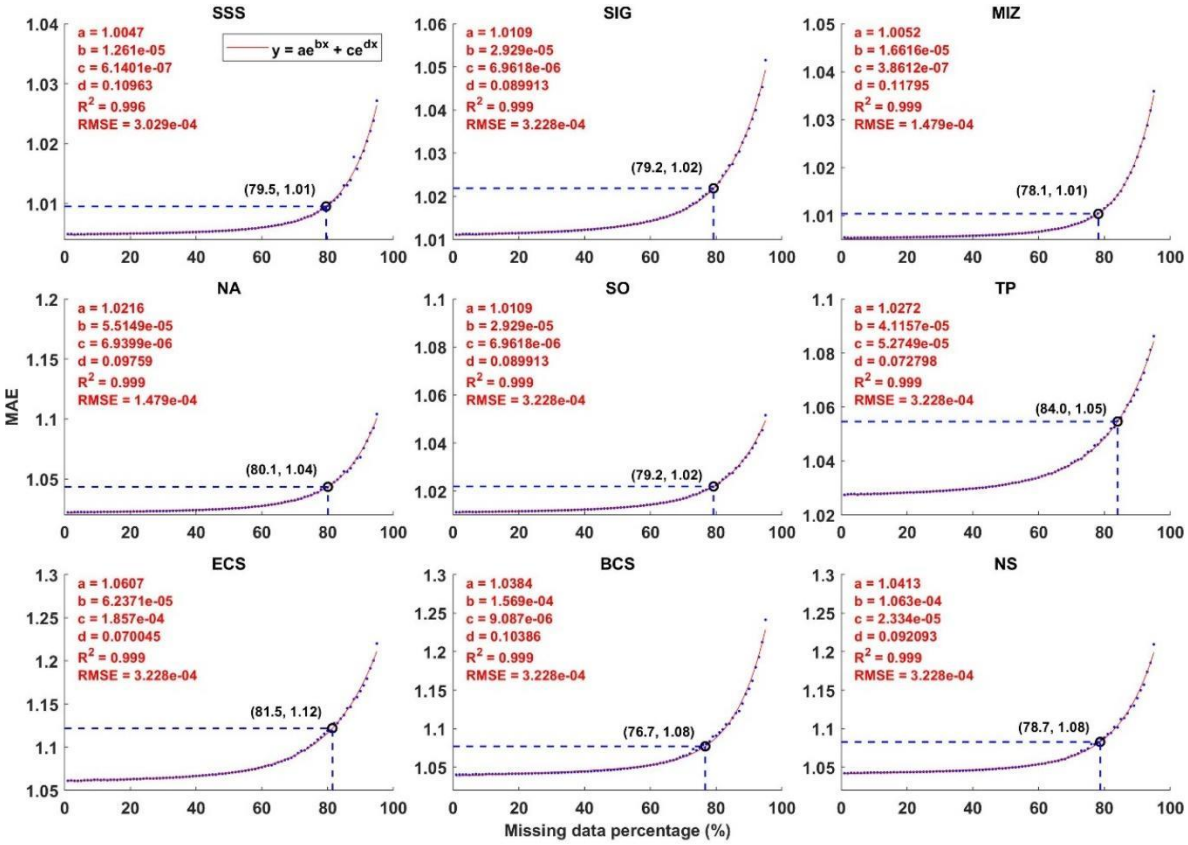

Fig. 3. Scatterplots of MAE vs percentage of missing data (PMD). The trendline (red line) is described by a two-term exponential model. The black circle indicates the value of PMD when the log10-transformed error increases by 100%.

To evaluate the performance using other metrics, we recreate a data matrix with 75% of missing data in each testing area. The results show r^2 is above 0.9, bias and slope are all around 1 (Figure 4). Based on these evaluations, we determine that 75% is a safe threshold as the percentage of missing pixels, where the DINEOF is reasonably applied.

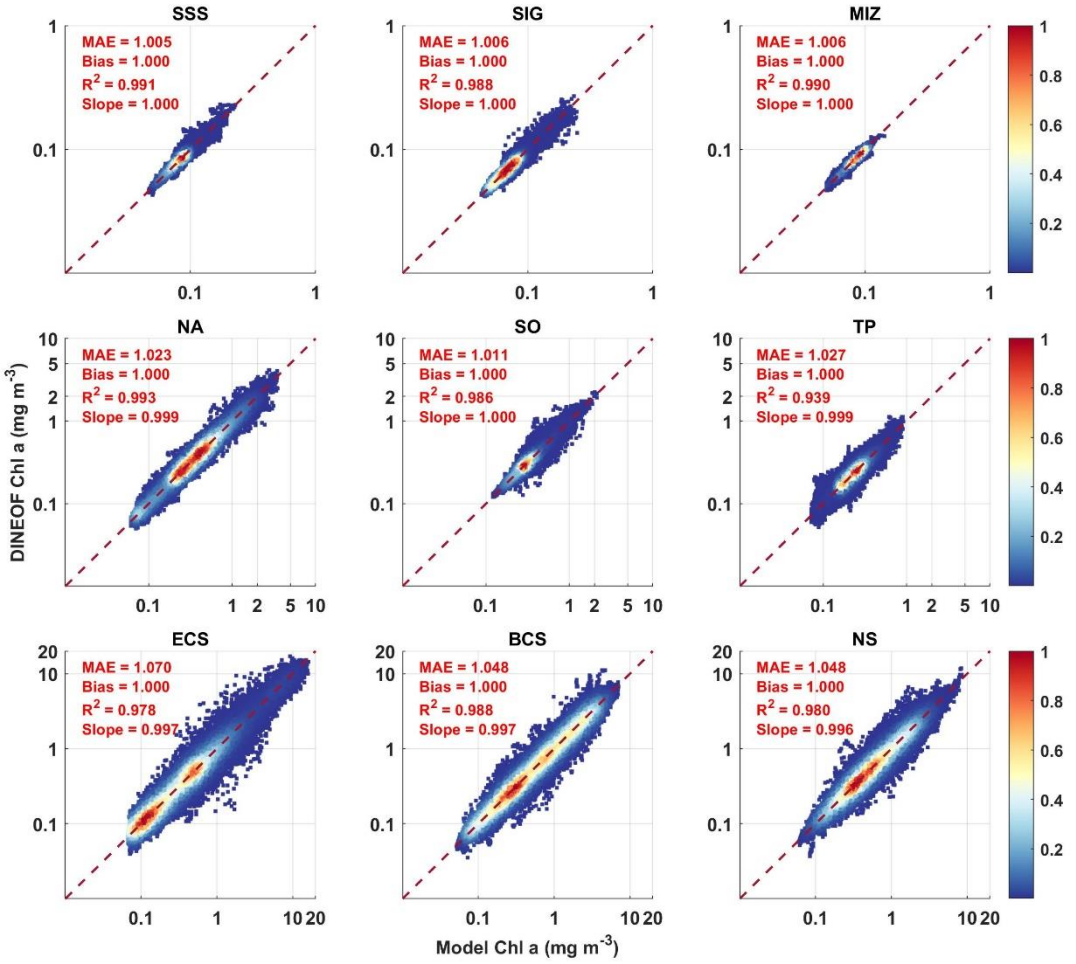

Fig. 4. Scatterplot of DINEOF reconstructed Chl *a* vs original model value. The percentage of missing data is 75% for all testing areas. The color represents data density. Red line = 1:1 ratio.

c. Impact of the distribution of missing data and validation of DINEOF+

To evaluate the impacts of the temporal and spatial distribution of missing data, a mask is created based on the global daily L3 MODIS-Aqua CHL product in 2019. The mask is applied to the model-derived Chl *a* so that incomplete dataset can have the same sparsity pattern as observed in the real satellite data.

Compared to random distribution, the gaps derived from satellite data result in higher MAE of reconstructed data in all testing areas when PMD are the same (Table 3). The increases of MAE in the mesotrophic and eutrophic regions are generally one magnitude greater than in the oligotrophic regions. In addition, the mean square error of initial

incomplete data does not show any correlation to the MAE. Therefore, we assert that the increased error is attributed to the difference in sparsity patterns.

Table 3. Statistic of data reconstruction in testing areas when the missing data is distributed in random and real satellite data in 2019. $\|\cdot\|_F$ denote Frobenius norm. * indicates that the calculation is based on log10-transform.

		Gaps in random		Gaps as is satellite data	
Testing areas	PMD (%)	$\|\Delta\|_F^2/n$	MAE*	$\|\Delta\|_F^2/n$	MAE*
SSS	66.95	0.004	1.004	0.004	1.007
SIG	70.62	0.003	1.006	0.003	1.008
MIZ	72.23	0.005	1.006	0.005	1.011
NA	87.51	0.226	1.038	0.228	1.072
SO	85.20	0.088	1.015	0.087	1.034
TP	75.56	0.043	1.027	0.041	1.048
ECS	82.94	0.621	1.092	0.691	1.163
BCS	82.19	2.195	1.091	1.915	1.245
NS	74.32	0.671	1.052	0.645	1.106

Furthermore, we selected the test data of the BCS as an example to analyze the characteristics of the distribution of missing data and errors in the reconstructed matrix. After removing null rows and columns, the overall PMD is 72.02%. The missing data is unevenly distributed in the data matrix where the column-based PMD ranges from 0.03 to 52.19% (Figure 5a). This is consistent with the fact that persistent cloud cover results in a large percentage of missing data in some areas during a year. The absolute error matrix shows a great variance of errors in the reconstructed missing data (Figure 5a). Large errors are highlighted in red and yellow color between the row 1600 and row 1200. The r^2 and slope are reduced to 0.508 and 0.683 respectively (Figure 5b) compared to 0.998 and 0.997 when the missing data is randomly distributed (Figure 4). After the use of the connectivity filter, these pixels of large errors are successfully identified and removed from the reconstructed matrix (Figure 5c), and thus significantly improve the overall accuracy (Figure 5d).

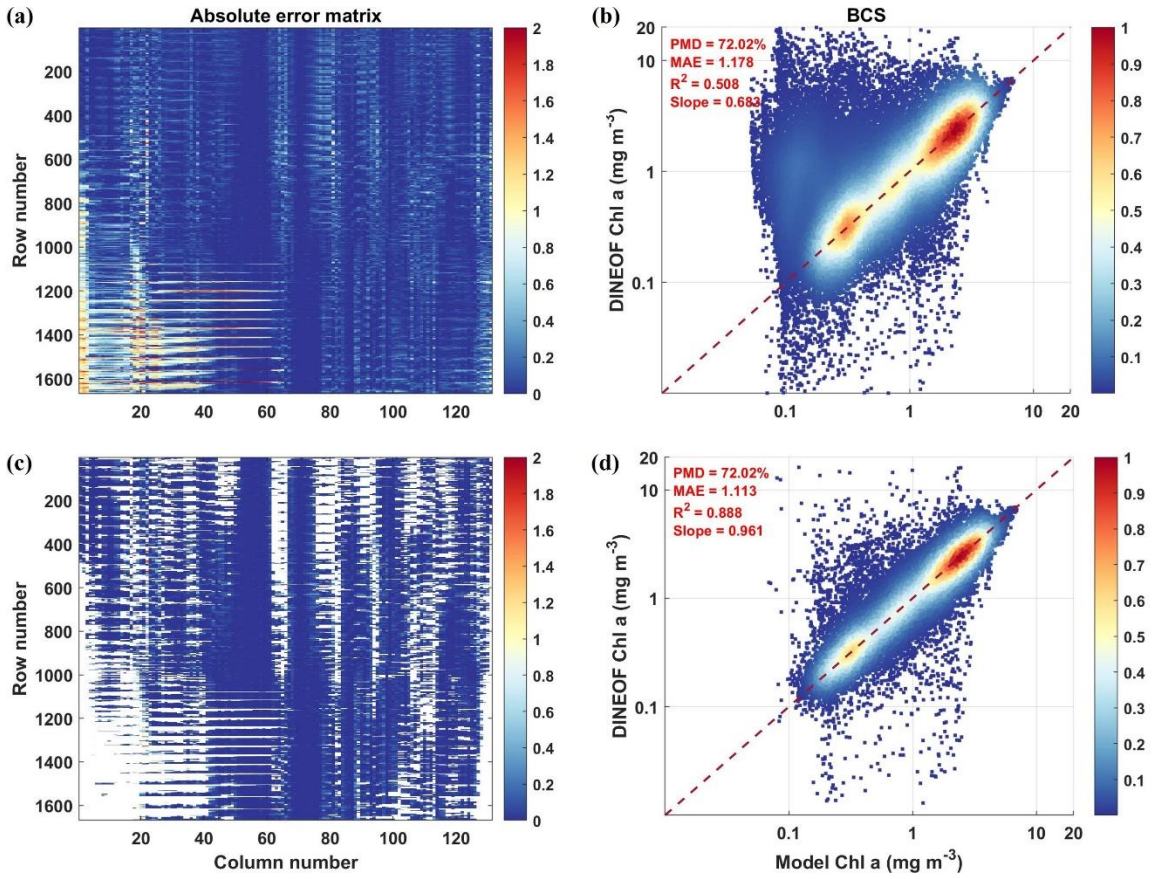

Fig. 5. The left two panels are absolute errors of DINEOF reconstructed Chl *a* before (a) and after (c) connectivity filter is applied in the BCS. Values are log-transformed prior to the calculation of errors. White indicates no data. The right two panels are scatterplots of DINEOF reconstructed data vs original model value before (b) and after (d) connectivity filter is applied. The color indicates data density. Red line = 1:1 ratio.

We compared the results of all test areas reconstructed by DINEOF with and without connectivity filter (Figure 6). Measured by r^2, MAE, and slope, the performance of DINEOF is least affected by missing data in three oligotrophic regions (Figure 6a). In the TP, ECS and BCS, the r^2 is below 0.9. It is obvious that the effect of gaps in real satellite data decreases the accuracy of reconstructed data particularly in the eutrophic regions. After the use of connectivity filter, the r^2 increased from 0.752 to 0.823 in the TP, from 0.883 to 0.923 in the ECS and from 0.419 to 0.896 in the BCS. MAE and slope are also improved in all test areas (Figure 6b).

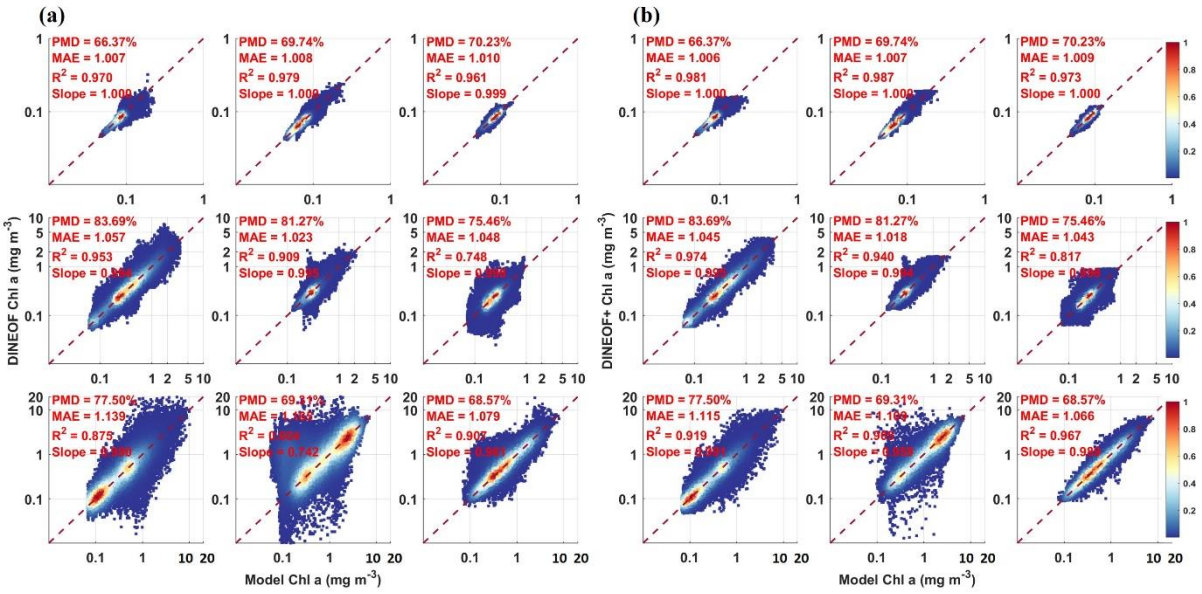

Fig. 6. Scatterplot of DINEOF reconstructed Chl *a* and original model value before (a) and after (b) connectivity filter is applied. The distribution of missing data has the same temporospatial pattern as daily L3 MODIS-Aqua Chl *a* product in 2019 where the mask was obtained. The minimum percentage of missing data is 6% in each column and row. The color indicates data density. Red line = 1:1 ratio.

4. Application to OC-CCI global daily Chl *a* product

To demonstrate how DINEOF+ behaves on real satellite data, we now use a multi-sensor dataset in 2019 obtained from the ESA Ocean Color Climate Change initiative (OC-CCI) (https://www.oceancolour.org/) (Sathyendranath et al. 2019). It consists of 365 days' images at 4 km resolution over the global ocean. In this study, we exclude coastal waters and delineate the open ocean into 21 subregions based on the biome boundaries (Figure A1). There are 2.88–11.27% of available pixels in the 7 polar biomes including the Baffin Bay, Greenland Sea, Hudson Bay, Kara Sea, Laptev Sea, Pacific Arctic and Southern Ocean south of 60ºS latitude (Table A1), 12.15–18.86% of data availability in the subpolar waters of North Atlantic, North Pacific and Southern Ocean, and 30.22–49.95% in oceans between 40ºN–50ºS mainly composed of oligotrophic waters.

As seen from the four sequenced images (Figure 7a, c, e, g), missing data is nonuniformly distributed across different ocean basins and dates. A consistently large number of missing data is found in the high-latitude regions including the North Atlantic, North Pacific and Southern Oceans. Consequently, it is almost impossible to detect the development of phytoplankton blooms in these regions throughout the year. By applying the DINEOF+ to

this data, it is shown that clear spatial patterns of Chl *a* distribution are obtained in the reconstructed images (Figure 7b, d, f, h). Noticeable spring blooms are observed in the Bering-Chukchi Sea, North Atlantic and Southern Oceans. Meanwhile, high Chl *a* concentrations are shown distributed along the equatorial Atlantic and eastern Pacific all year around. In September, a second bloom can be observed in the North Pacific and Atlantic Oceans (Figure 7h). Within these mesoscale structures, there are some sub-mesoscale features such as filaments and eddy-shaped Chl *a* blooms (Figure b, d, f, h) which are not visible in the original dataset due to the presence of gaps. The availability of daily data increases by 51% in the equatorial Pacific and Atlantic, and 43–55% in the oligotrophic regions including the gyres north and south of the equator and Indian Ocean (Table A1).

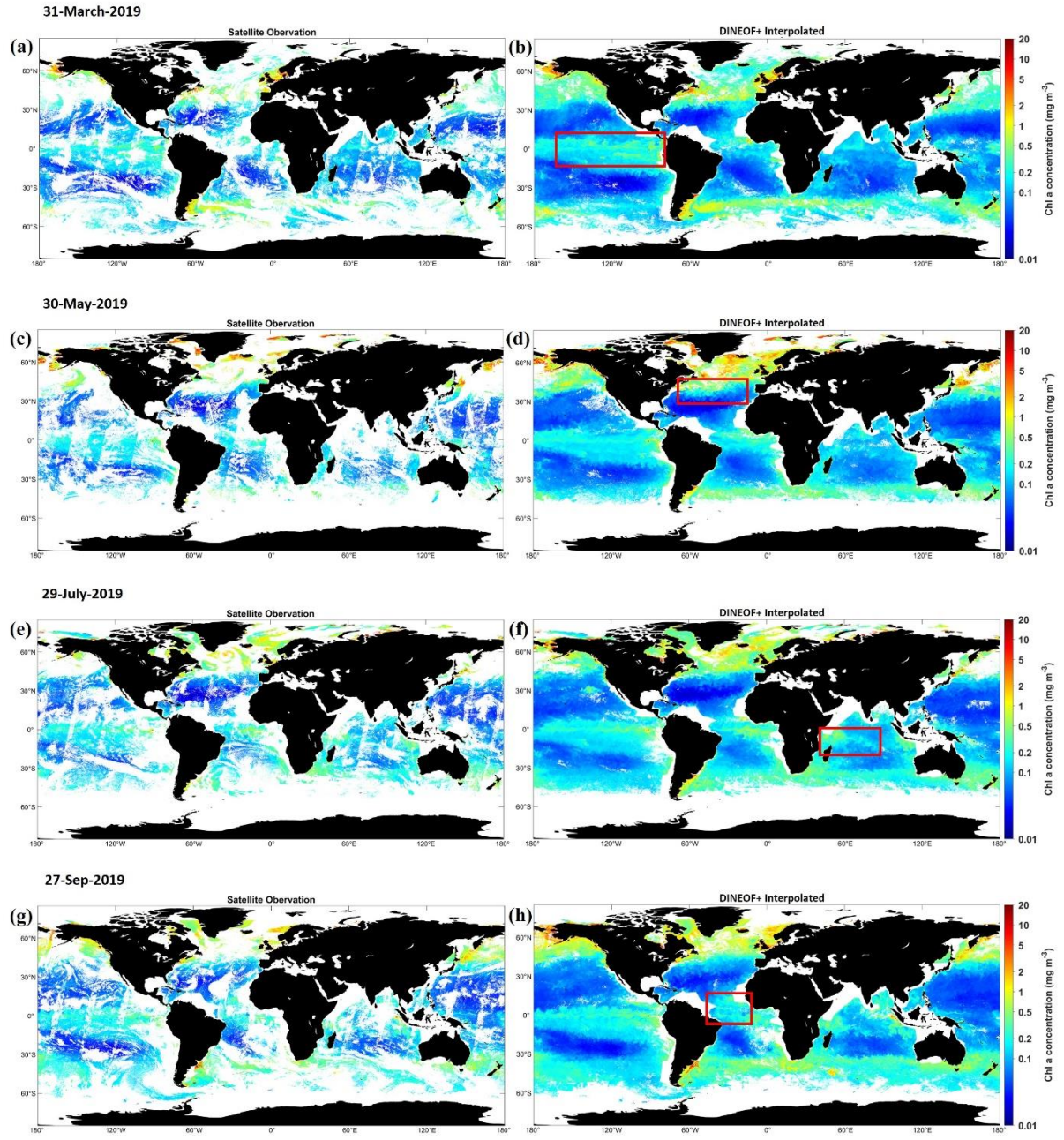

Fig. 7. Global daily Chl *a* concentration from level 3 daily ESA-CCI at 4 km resolution (left panels) and corresponding DINEOF+ reconstructed results (right panels) in 2019 on (a, b) March 31; (c, d) May 30; (e, f) July 29; (g, h) Sep 27. The red boxes indicate areas with sub-mesoscale features such as eddies and filaments. White color indicates no data.

Error maps associated with the reconstruction are given by using the method proposed by (Beckers et al. 2006). We use an error length of 29 km. The expected standard deviation ranges from 1 to 1.02 with exceptions of some points that reach 1.04 - 1.05 in the polar waters (Figure 8). Since the errors are within the range of regional MAE estimated from our validation, no further removal of points seems necessary.

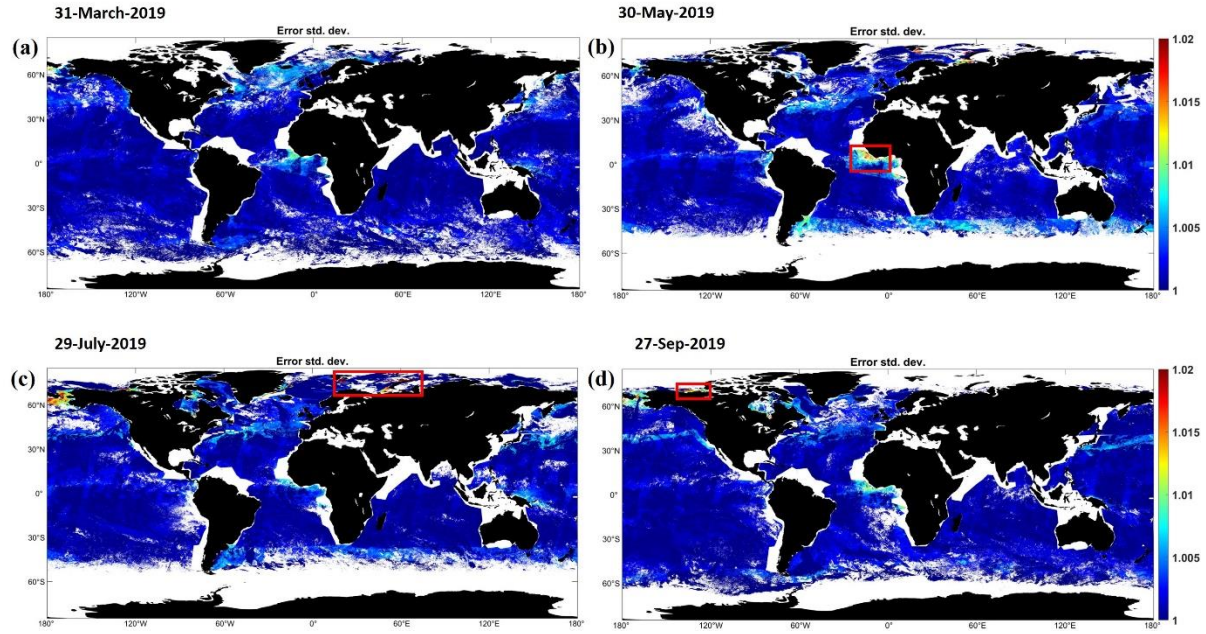

Fig. 8. The estimated error standard deviation for the DINEOF+ reconstruction in 2019 on (a) March 31; (b) May 30; (c) July 29; (d) Sep 27. The red boxes indicate areas with relatively higher error std. Values are log-transformed prior to the calculation of errors. White color indicates no data.

In addition to 2019, we also applied DINEOF+ to the global daily datasets from 2003 to 2020 for further confirming improvements on Chl *a* time series observation. The annual mean coverage of daily data on Chl *a* is 22.5% in the equatorial Atlantic, 28.92% in the equatorial Pacific, 11.77% in the subpolar North Atlantic, 12.62% in the subpolar North Pacific, 28.08% in the oligotrophic oceans and 4.49% in the polar oceans (Figure 9a). After we applied the method, the annual mean coverage increases to 60.9% in the equatorial Atlantic, 76.65% in the equatorial Pacific and 76.78% in the oligotrophic oceans (Figure 9b), though the availability of daily Chl *a* is still below 20% in subpolar and polar oceans. In the next section, we compare the reconstructed Chl *a* to *in situ* observations including two times-series data from Bermuda Atlantic Time-series Study (BATS) and Hawaii Ocean Time-series Station (HOTS). Both stations are located in the oligotrophic region where the annual mean data coverage reaches 76% in the reconstructed datasets (Figure 9b).

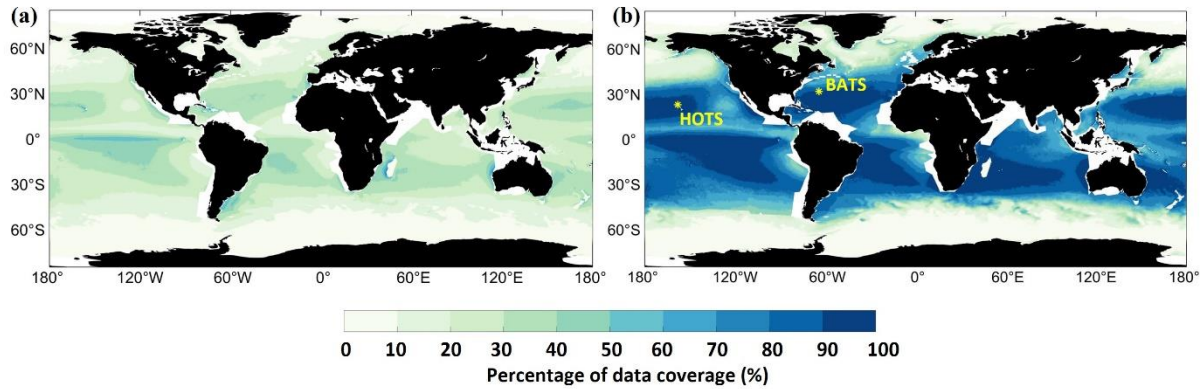

Fig. 9. Annual mean coverage of daily Chl *a* data during 2003–2020: (a) level-3 daily ESA-CCI at 4 km resolution; (b) Corresponding DINEOF reconstructed results. The data coverage is the percentage of available data in each pixel with regard to the total number of time steps. The location of BATS and HOTS are marked as asterisk in panel (b).

5. Validation: match-ups with *in situ* data

In this section, we perform validation of DINEOF+ interpolated Chl *a* via comparisons to *in situ* measurements. The *in situ* measurements are selected from SeaBASS during 2003–2020 (https://seabass.gsfc.nasa.gov/) that includes both fluorometric and HPLC-derived Chl *a*. The coincident satellite pixels are removed from datasets and are recovered by applying DINEOF+. The total number of matchups used for validation between *in situ* and reconstructed pixels is 858 located across the global ocean (Figure A2). Furthermore, we divide these matchups into oligotrophic, mesotrophic, and eutrophic waters according to the definition used in section 3.

Measured by MAE, r^2 and slope, the errors of DINEOF+ interpolated Chl *a* are quantitatively similar to the original satellite-derived Chl *a* across all waters (Figure 10a, e). DINEOF+ performs poorest in the eutrophic indicated by the r^2 and MAE (Figure 10h). However, similar error metrics are also found in the original satellite-derived Chl *a* (Figure 10d). Thus, we posit that the errors are mostly inherent differences between satellite-derived Chl *a* and *in situ* measurements. A similar performance is also shown in the oligotrophic (Figure 10b, f) and mesotrophic areas (Figure 10c, g). Although DINEOF+ reconstruction added noise to the original pixel values, it also helps reduce the error of abnormal measurements in the datasets as shown in our examples (Figure 10a, c and Figure 10d, h).

Figure 11 allows a comparison of *in situ* surface Chl *a* (SChl *a*) evolution (blue curve) with the satellite retrieved concentrations on the 8-day average (red curve) and DINEOF+ daily resolution (yellow curve) over their overlapping period during 2003–2020. It shows that both satellite and DINEOF+ derived signals agree well with the *in situ* observations of SChl *a* at BATS in terms of seasonal pattern, annual variation and magnitude. At HOTS, SChl *a* concentration is underestimated by the coincident satellite measurements over the periods while the DINEOF+ daily time series exhibit a better agreement with the *in situ* SChl *a* indicated by a higher correlation coefficient (Figure 11b, d). Furthermore, the DINEOF daily time series includes more measurements within a weekly scale (Figure 3A) and thus provides reasonable Chl *a* evolution such as the timing of bloom peaks.

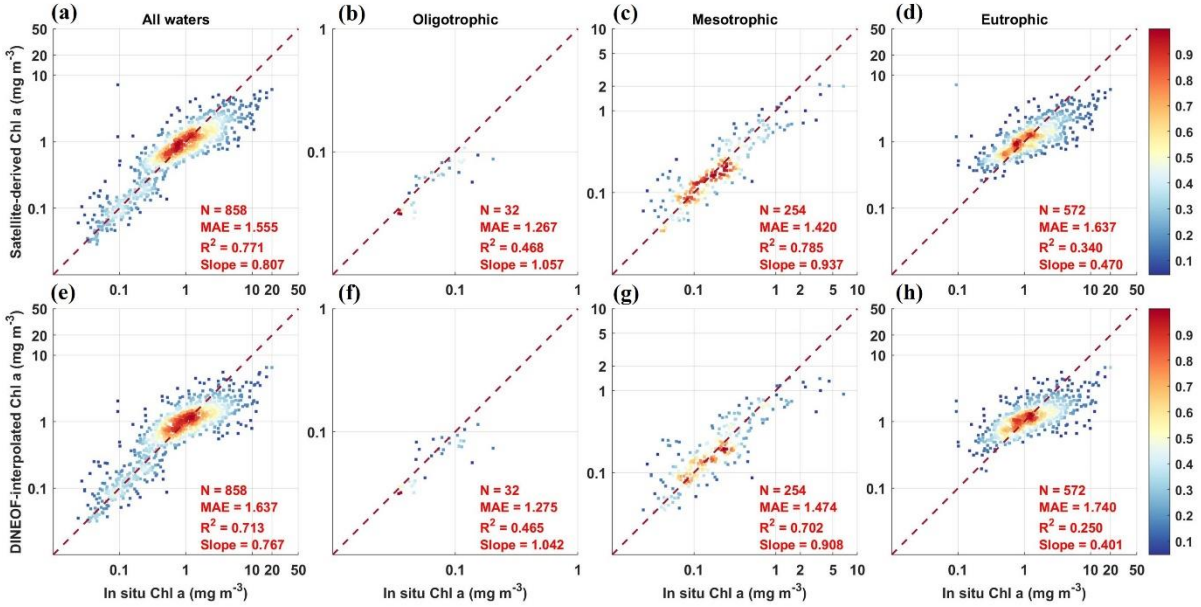

Fig. 10. Scattering plots of original satellite-derived vs *In situ* Chl *a* (top panel) and DINEOF+ interpolated vs *In situ* Chl *a* (bottom panel): (a, e) Across all water types, (b, f) Oligotrophic, (c, g) Mesotrophic, (d, h) Eutrophic. N is the number of match-ups. Red line = 1:1 ratio.

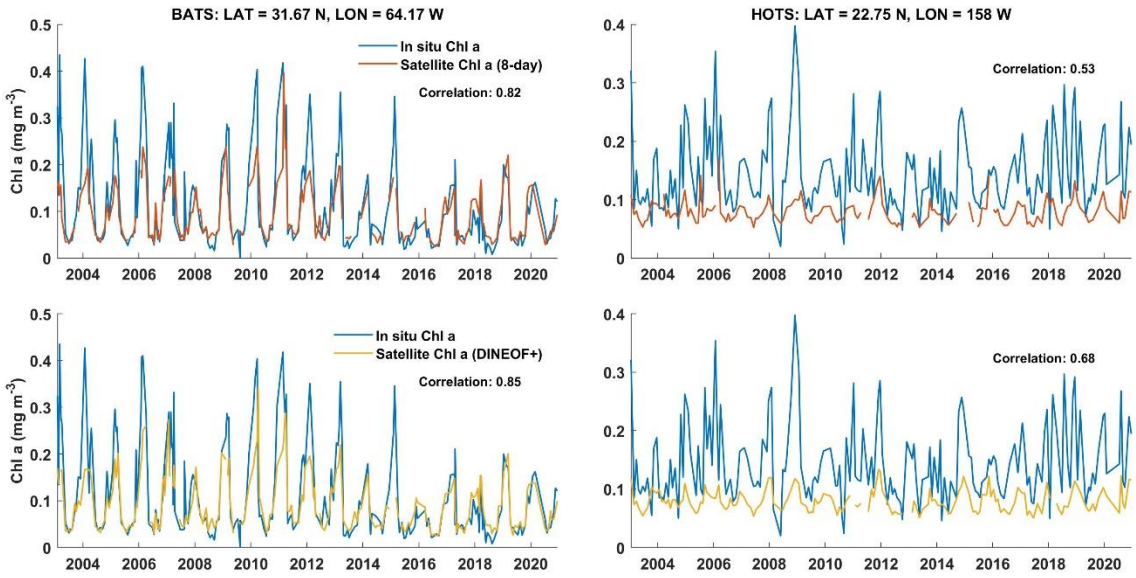

Fig. 11. Comparison of *in situ* surface Chl *a* time series (blue curves) to 8-day average ESA OC-CCI Chl *a* time series (red curves) and DINEOF-reconstructed Chl *a* time series (yellow curves). The *in situ* measurements are located at BATS (a, c) and HOTS (b, d).

6. Discussion

Due to persistent gaps in satellite observations, it is challenging to interpret phytoplankton dynamics in time and space using ocean color data. Previous studies have shown that the DINEOF algorithm is an efficient method for recovering missing data of geophysical variables such SST and SSS. In this study, we improve the DINEOF algorithm by integrating connectivity filter (i.e. DINEOF+) and provide a comprehensive validation of the reconstructed Chl *a* by comparison to both simulated and *in situ* measurements.

Our validation confirms that both the total number and distribution pattern of missing data are related to the accuracy of recovered missing data. According to the theory of matrix completion, unknown entries from a matrix are not guaranteed to be recovered unless a sufficient number of them are observed, and these samples are uniformly random (Candès & Recht, 2009). This raises certain requirements for the datasets that need to be recovered. In terms of the number of missing data, we show that 75% of PMD is a threshold for performing DINEOF+. In real satellite images, data gaps are not uniformly distributed and the PMD often reaches above 75% particularly in high latitude and coastal regions. It is useful to skip some days and pixels to reduce the overall PMD of a data matrix. Our validation also shows that the real data gaps will impair the accuracy of reconstructed values compared to the tests based on random samplings (Table 3). Although we cannot define a quantitative criterion to

determine which distribution of gaps allows a data reconstruction, the connectivity filter works as an effective method of removing highly biased values by examining the condition of data availability neighboring each pixel since the physical correlation with ad valid neighbor is generally stronger than with a point much further away. Users can change the size of neighboring structures (Figure 1) according to the study areas. Future studies may consider designing a weighted structure using pixels of different length scales.

In addition to missing data, the influence of variance or heterogeneity of the dataset also needs to be considered for applying DINEOF+. In our experiments, we observed much higher errors in the eutrophic regions (i.e., ECS, BCS, NS) compared to mesotrophic and oligotrophic regions (Table 3). This indicates that the reconstruction of Chl *a* values will have larger uncertainties in those regions that are characterized by greater variance in time and space. Typical examples include most coastal oceans where Chl *a* is characterized by high variance throughout a year (O'Reilly & Werdell, 2019). This implies the need for caution when applying DINEOF+ to reconstruct Chl *a* in these regions. Nevertheless, DINEOF+ demonstrates its strength in recovering the development of phytoplankton blooms characterized by a high spatial heterogeneity of Chl *a* concentration.

For global applications, previous studies simply divided the entire oceans into subareas by latitude to increase the efficiency of implementing DINEOF (Liu & Wang, 2018, 2019). Here, we argue that this is not an appropriate method regarding the high heterogeneity of Chl *a* in the upper ocean. Fay and McKinley (2014) defined 17 open-ocean biomes classified according to observations of Chl *a*, SST and MLD. Using these biomes provides a basis for an alternative method applying DINEOF+ for reconstructing Chl *a* dataset. Our results improve the daily Chl *a* coverage by 26.86% for the global open oceans during 2003–2020. When using biomes-based reconstruction several properties need to be considered: first, it excludes coastal regions which tend to have very high variance of Chl *a*; second the biomes are classified based on biogeochemical functions and thus exhibit more consistent changes in Chl *a* through a year; third, it provides a mean to apply and compare reconstructed datasets for biome-scale studies on phytoplankton dynamics and primary production. It should be noted that the recovery rate varies with ocean basins and years, depending on the data availability in the original dataset. In the oligotrophic oceans between 40°N–40°S, the daily Chl *a* coverage increased by 43–55% on average, which provides us with a nearly complete daily Chl *a* time series at single pixel level for decades (Figure A3). In contrast, there is only

4.66% of the increase in the polar oceans. To obtain higher data coverage in high-latitude oceans, we suggest applying DINEOF+ to a composite dataset such as 8-day running mean.

The potential applications of DINEOF+ extend beyond the specific dataset on Chl *a*. Figure 12 illustrates an example of applying DINEOF+ to datasets on Remote Sensing Reflectance (Rrs) at 443 nm. Using DINEOF+ greatly increased the data coverage of daily Rrs product. As a fundamental parameter used in ocean color remote sensing, the reconstructed Rrs product can be used to derive other ocean color datasets on parameters such as Chl *a*, Colored Dissolved Organic Matter (CDOM), and Particulate Organic Carbon (POC).

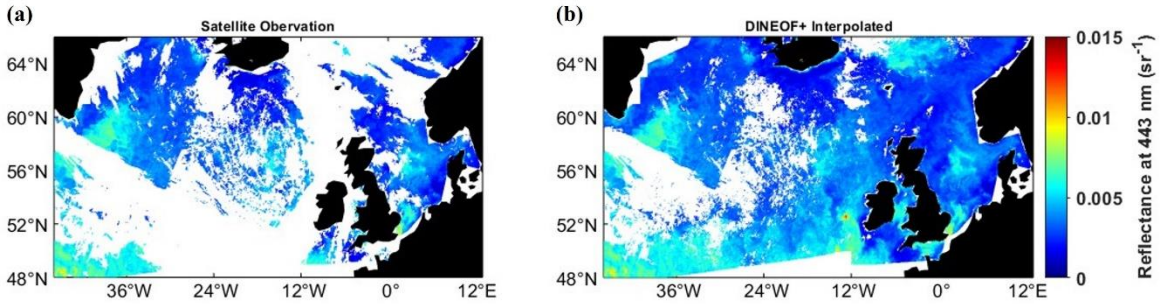

Fig. 12. Remote sensing reflectance at 443 nm in the North Atlantic Ocean from level 3 daily ESA-CCI product at 4 km resolution (left panels) and corresponding DINEOF+ reconstructed results (right panels) on 12 Sep 2022. White color indicates no data.

7. Concluding remarks

We demonstrate that DINEOF+ is a useful technique that allows us to obtain an unprecedented high-temporal resolution ocean color dataset. Using this dataset will unequivocally enhance our ability to interpret the natural variability of surface Chl *a* concentration that is dominated by high-frequency fluctuations at small spatial scales (Keerthi et al. 2022). Temporal resolution of the dataset also influences determining phenological metrics of phytoplankton such as the timing of bloom initiation and peaks. Because DINEOF+ can effectively increase the temporal resolution of Chl *a* time series for one year it will reduce the uncertainty resulting from the original data gaps.

For readers of interest, we summarize the main steps of DINEOF+ below:

Step 1) Organize sequences of selected images into a 2-D matrix $\mathbf{X}_o$ where each column represents measurements on a particular day and each row is a time series of measurements at a pixel location.

Step 2) Subtract an average value from $\mathbf{X}_o$ and set aside randomly at least 30 data points for cross-validation to determine the optimal number of EOFs. Meanwhile, all missing values are initialized as zero.

Step 3) If the PMD of $\mathbf{X}_o$ is greater than 75%, remove some columns and rows until PMD is equal or less than 75%.

Step 4) Calculate the EOF series by using SVD of $\mathbf{X}_o$.

Step 5) Starting from $N = 1$, update missing data with truncated EOF series which consists of the first N EOFs

Step 6) Repeat steps (3)–(4) until convergence occurs and then calculate error estimations.

Step 7) Increase the number of EOFs until the error estimation begins to increase.

Step 8) Apply connectivity filter to the updated matrix.

Acknowledgments.

We thank ESA OC-CCI group for the data availability, production and maintenance for the ocean color data used in this manuscript. We also thank the scientists and crewmembers for running the BATS (NSF OCE-1756105 and OCE-2122606) and HOT Time-series project over the last three decades.

Parts of this research were supported by NASA ROSES project (sponsor award #210319602) and Japan Aerospace Exploration Agency (JAXA) Global Change Observation Mission-Climate, GCOM-C (contracts #22RT000298) to AM.

Data Availability Statement.

This study has been conducted using E.U. Copernicus Marine Service Information; https://doi.org/10.48670/moi-00019 and https://doi.org/10.48670/moi-00282. Datasets from HOTS and BATS are accessible through https://hahana.soest.hawaii.edu/hot/hot-dogs/interface.html and https://bats.bios.asu.edu/data/.

The code of DINEOF+ used in this manuscript can be found in GitHub repository https://github.com/zhprm1992/DINEOF-plus.git

APPENDIX A

Application to global biomes and validation

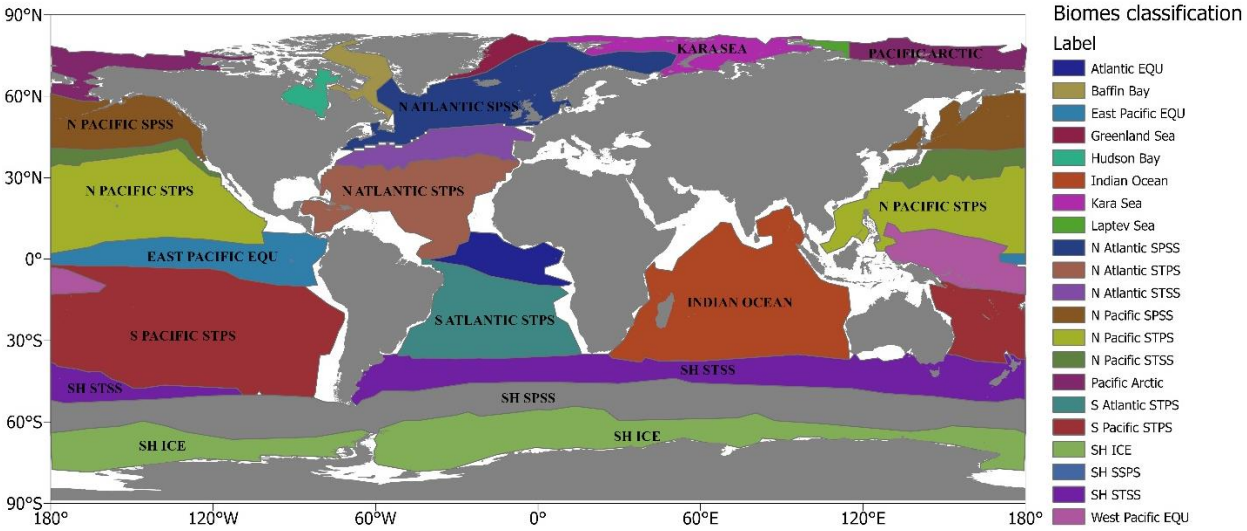

Figure A1. Global open-ocean biomes. The base map is created by Fay and McKinley (2014). ICE: ice biome; SPSS: subpolar seasonally stratified biome; SPSS: subtropical seasonally stratified biome; STPS: subtropical permanently stratified biome; EQU: equatorial biome. White indicated ocean areas that do not fit the criteria for any biome and are excluded from further analysis.

NO.		Daily Chl *a*	DINEOF daily Chl *a*	8-day Chl *a*
1	Atlantic EQU	43.55%	94.59%	95.27%
2	N Atlantic STPS	54.05%	97.53%	97.81%
3	N Atlantic STSS	32.82%	86.02%	86.44%
4	Baffin Bay	11.27%	27.90%	31.45%
5	E Pacific EQU	49.95%	95.30%	95.57%
6	Greenland Sea	4.77%	8.97%	17.21%
7	Hudson Bay	8.85%	20.89%	25.35%
8	Indian Ocean	48.95	95.10%	95.52%
9	Kara Sea	4.55%	7.40%	16.91%

10	Laptev Sea	2.88%	3.80%	11.54%
11	N Atlantic SPSS	14.99%	38.45%	51.77%
12	N Pacific SPSS	18.86%	48.95%	65.69%
13	Pacific Arctic	4.91%	8.58%	17.60%
14	N Pacific STPS	47.32%	95.10%	95.63%
15	N Pacific STSS	30.22%	85.34%	86.03%
16	S Pacific STPS	42.84%	91.81%	92.48%
17	SH ICE	3.28%	3.60%	15.70%
18	S Atlantic STPS	48.84%	95.37%	95.89%
19	SH SPSS	12.15%	26.90	49.04%
20	SH STSS	27.51%	79.51%	80.47%
21	W Pacific EQU	40.61%	92.02%	93.07%

Table A1. The percentage of available daily Chl *a* pixels in each biome in 2019.

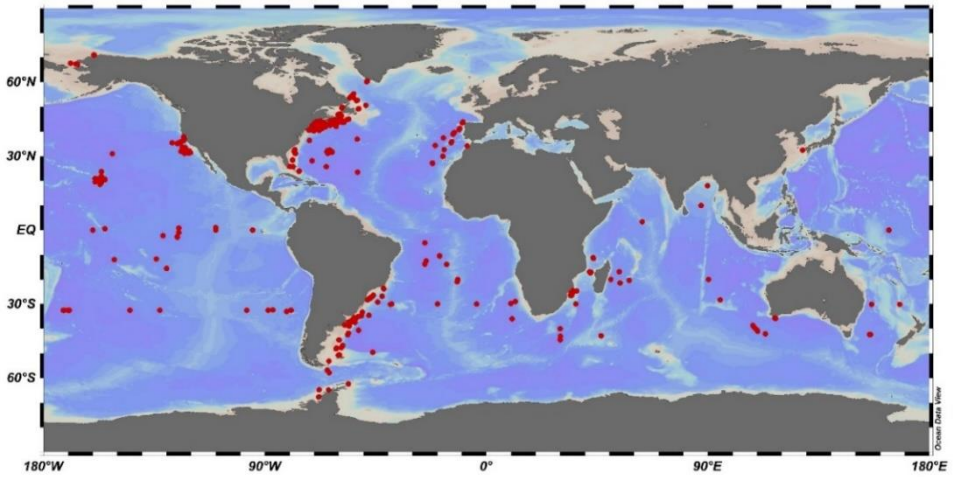

Figure A2. Geographic locations of in situ datasets used for validation of DINEOF reconstruction. Red dots are *in situ* Chl *a* measurements retrieved from SeaBASS.

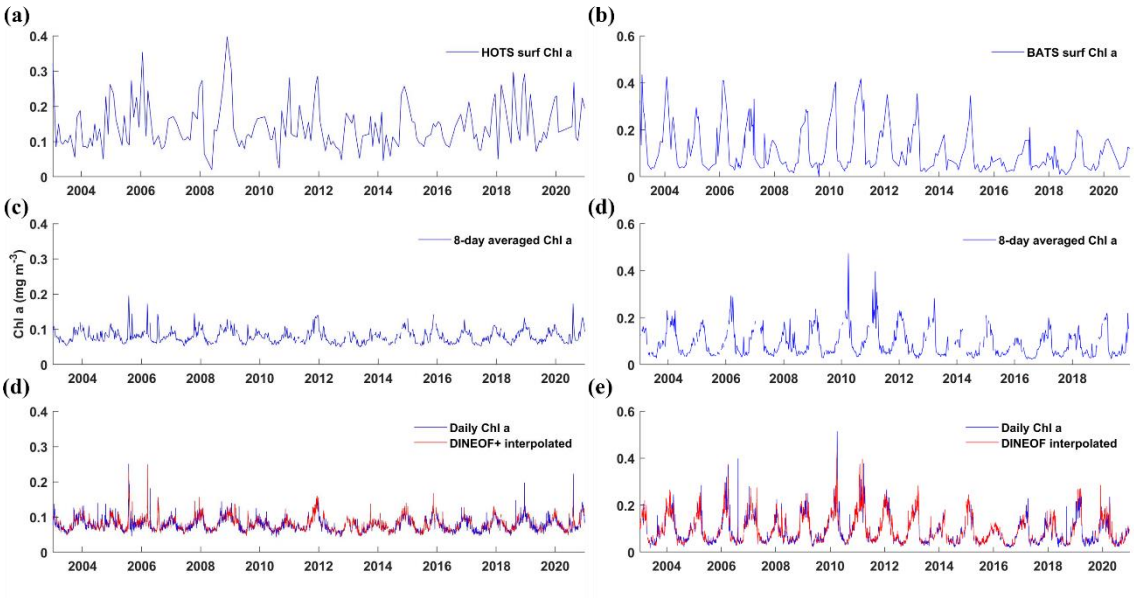

Figure A3. Chl *a* time series from 2003 to 2020. Left panels are HOTS *in situ* surf Chl *a* (a), and satellite matchup of 8-day average Chl *a* (c) and DINEOF-interpolated daily Chl *a* (d). Right panels are BATS *in situ* surf Chl *a* (b), and satellite matchup of 8-day average Chl *a* (d) and DINEOF-interpolated daily Chl *a* (e).

APPENDIX B

The theoretical foundation for convergence properties of DINEOF

DINEOF can be regarded as an approach of using maximum likelihood estimation (MLE) to solve a latent-variable model. The iteration of SVD is essentially a practical application of the Expectation-Maximization (EM) algorithm when we assume the original incomplete data matrix can be represented by a linear model plus noise with a Gaussian distribution.

This section provides the theoretical foundation of DINEOF and proof of its most important property of convergency that makes DINEOF a useful approach to reconstruct an incomplete data matrix.

a. Best k-dimension linear model

Denote data matrix as $\mathbf{A}$ containing observations. $\mathbf{A}_{ij}$ represents the value of the field $f(r,t)$ at location r_i and moment t_i:

$$\mathbf{A}_{ij} = f(r_i, t_j) \tag{B1}$$

Define $\mathbf{X}$ as a low-dimension linear matrix that approximates $\mathbf{A}$. Thus $\mathbf{A}_{ij}$ is equal to $\mathbf{X}_{ij}$ plus an error.

$$\mathbf{A}_{ij} = \mathbf{X}_{ij} + \delta \tag{B2}$$

We assume the error is from Gaussian distribution with zero mean and standard deviation δ, thus $\mathbf{A}_{ij} \sim N(\mathbf{X}_{ij}, \delta)$

We regard $\mathbf{X}_{ij}$ as a parameter, thus the log-likelihood of $\mathbf{A}_{ij}$ is

$$\log\Pr(\mathbf{A}_{ij}|\mathbf{X}_{ij}) = -\frac{1}{2\sigma^2}(\mathbf{A}_{ij} - \mathbf{X}_{ij})^2 + C \tag{B3}$$

Maximize $\log P(\mathbf{A}|\mathbf{X})$ is equivalent to minimize $\|\mathbf{A} - \mathbf{X}\|_F^2$, where $\|.\|_F$ is Frobenius Norm. Let $\mathbf{A} = \mathbf{U\Sigma V}$ be the singular value decomposition. Given the Eckart-Young theorem,

$$\min_{rank(\tilde{X}) \le k} \|\mathbf{A} - \mathbf{X}\|_F^2 = \left\|\mathbf{A} - \mathbf{U}_k\mathbf{\Sigma}_k\mathbf{V}_k^T\right\|_F^2 \tag{B4}$$

Where $\mathbf{U}_k$ is the top *k* left singular vectors, $\mathbf{\Sigma}_k$ is the diagonal matrix with entries of top *k* singular values, $\mathbf{V}_k$ is the top *k* right singular vectors.

Thus, the best *k*-rank approximation to $\mathbf{A}$ is given by $\mathbf{X} = \mathbf{U}_k\mathbf{\Sigma}_k\mathbf{V}_k^T$ when $\mathbf{A}$ is a complete data matrix.

b. Approximation to incomplete data matrix

Iteration of implementing SVD is the key step in DINEOF operation and is belonging to an EM procedure, which can prove its properties such as convergence and approximation of unknown data.

Incomplete matrix $\mathbf{A}$ comprises two parts: observed data, $\mathbf{A}^o$ and unobserved data $\mathbf{A}^u$. The complete log-likelihood is given by

$$\log \mathrm{P}(\mathbf{A}^o, \mathbf{A}^u|\mathbf{X}) = \sum_{\mathbf{A}_{i,j}\epsilon\mathbf{A}^o} \log\mathrm{P}\left(\mathbf{A}_{ij}|\mathbf{X}\right) + \sum_{\mathbf{A}_{i,j}\epsilon\mathbf{A}^u} \log\mathrm{P}\left(\mathbf{A}_{ij}|\mathbf{X}\right) \tag{B5}$$

In the *t*th iteration of E-step, the posterior distribution of $\mathbf{A}^u$ is $q^{(t)}(\mathbf{A}^u) = \sum_{\mathbf{A}_{i,j}\epsilon\mathbf{A}^u} \mathrm{P}\left(\mathbf{A}_{ij}|\mathbf{X}^{(t-1)}\right)$.

The expectation of complete log-likelihood with respect to $\mathbf{A}^u$ is expressed as:

$$E_{q^{(t)}}\left(\sum_{\mathbf{A}_{i,j}\epsilon\mathbf{A}^o} \log\mathrm{P}\left(\mathbf{A}_{ij}|\mathbf{X}^{(t)}\right) + \sum_{\mathbf{A}_{i,j}\epsilon\mathbf{A}^u} \log\mathrm{P}\left(\mathbf{A}_{ij}|\mathbf{X}^{(t)}\right)\right)$$

$$= \sum_{\mathbf{A}_{i,j}\epsilon\mathbf{A}^o} \log\mathrm{P}\left(\mathbf{A}_{ij}|\mathbf{X}^{(t)}\right) + E_{q^{(t)}}\left(\sum_{\mathbf{A}_{i,j}\epsilon\mathbf{A}^u} \log\mathrm{P}\left(\mathbf{A}_{ij}|\mathbf{X}^{(t)}\right)\right) \tag{B6}$$

Here,

$$\sum_{\mathbf{A}_{i,j}\epsilon\mathbf{A}^o} \log\mathrm{P}\left(\mathbf{A}_{ij}|\mathbf{X}^{(t)}\right) = -\frac{1}{2\sigma^2}\left(\mathbf{A}_{ij} - \mathbf{X}_{ij}^{(t)}\right)^2 + C \tag{B7}$$

$$E_{q^{(t)}}\left(\log\mathrm{P}\left(\mathbf{A}_{ij}|\mathbf{X}^{(t)}\right)\right)$$

$$= -\frac{1}{2\sigma^2} E_{q^{(t)}}\left(\left(\mathbf{A}_{ij} - \mathbf{X}_{ij}^{(t)}\right)^2\right) + C$$

$$= -\frac{1}{2\sigma^2}\left(E_{q^{(t)}}(\mathbf{A}_{ij}^2) - E_{q^{(t)}}\left(2\mathbf{A}_{ij}\mathbf{X}_{ij}^{(t)}\right) + E_{q^{(t)}}\left(\mathbf{X}_{ij}^{(t)}\right)^2\right) + C$$

$$= -\frac{1}{2\sigma^2}\left((\mathbf{X}_{ij}^{(t-1)})^2 - \delta^2 + 2\mathbf{X}_{ij}^{(t-1)}\mathbf{X}_{ij}^{(t)} + \left(\mathbf{X}_{ij}^{(t)}\right)^2\right) = -\frac{1}{2\sigma^2}\left(\mathbf{X}_{ij}^{(t-1)} - \mathbf{X}_{ij}^{(t)}\right)^2 + C \tag{B8}$$

Thus, the expectation of the complete log-likelihoods can be written as

$$-\frac{1}{2\sigma^2}\left(\sum_{\mathbf{A}_{i,j}\epsilon\mathbf{A}^o}\left(\mathbf{A}_{ij} - \mathbf{X}_{ij}^{(t)}\right)^2 + \sum_{\mathbf{A}_{i,j}\epsilon\mathbf{A}^u}\left(\mathbf{X}_{ij}^{(t-1)} - \mathbf{X}_{ij}^{(t)}\right)^2\right) + C \tag{B9}$$

Unobserved $\mathbf{A}_{ij}$ is filled with $\mathbf{X}_{ij}^{(t-1)}$ at time *t*. The maximum expectation is equivalent to

$$\underset{\mathbf{X}}{\operatorname{argmin}} \sum \left(\mathbf{A}_{ij} - \mathbf{X}_{ij}^{(t)}\right)^2$$

Thus, the optimal value $\mathbf{X}_{ij}^{(t)}$ can be obtained by performing SVD on $\mathbf{A}^t$.

The EM procedure is ensured to converge. Thus, DINEOF estimated values of missing data are ensured to converge.

REFERENCES

Alvera-Azcárate, A., A. Barth, M. Rixen, and J. M. Beckers, 2005: Reconstruction of incomplete oceanographic data sets using empirical orthogonal functions: application to the Adriatic Sea surface temperature. *Ocean Modelling*, **9,** 325-346, https://doi.org/10.1016/j.ocemod.2004.08.001.

Alvera-Azcárate, A., A. Barth, J.-M. Beckers, and R. H. Weisberg, 2007: Multivariate reconstruction of missing data in sea surface temperature, chlorophyll, and wind satellite fields. *Journal of Geophysical Research: Oceans*, **112**, https://doi.org/10.1029/2006JC003660.

Alvera-Azcárate, A., A. Barth, G. Parard, and J.-M. Beckers, 2016: Analysis of SMOS sea surface salinity data using DINEOF. *Remote Sensing of Environment*, **180,** 137-145, https://doi.org/10.1016/j.rse.2016.02.044.

Antoine, D., J.-M. André, and A. Morel, 1996: Oceanic primary production: 2. Estimation at global scale from satellite (Coastal Zone Color Scanner) chlorophyll. *Global Biogeochemical Cycles*, **10,** 57-69, 10.1029/95GB02832.

Aumont, O., C. Ethé, A. Tagliabue, L. Bopp, and M. Gehlen, 2015: PISCES-v2: an ocean biogeochemical model for carbon and ecosystem studies. *Geosci. Model Dev.*, **8,** 2465-2513, 10.5194/gmd-8-2465-2015.

Beckers, J. M., and M. Rixen, 2003: EOF Calculations and Data Filling from Incomplete Oceanographic Datasets. *Journal of Atmospheric and Oceanic Technology*, **20,** 1839-1856, 10.1175/1520-0426(2003)020<1839:ECADFF>2.0.CO;2.

Beckers, J. M., A. Barth, and A. Alvera-Azcárate, 2006: DINEOF reconstruction of clouded images including error maps – application to the Sea-Surface Temperature around Corsican Island. *Ocean Sci.*, **2,** 183-199, 10.5194/os-2-183-2006.

Behrenfeld, M. J., and E. S. Boss, 2014: Resurrecting the Ecological Underpinnings of Ocean Plankton Blooms. *Annual Review of Marine Science*, **6,** 167-194, 10.1146/annurev-marine-052913-021325.

Behrenfeld, M. J., and Coauthors, 2006: Climate-driven trends in contemporary ocean productivity. *Nature*, **444,** 752-755, 10.1038/nature05317.

Benedetti, F., M. Vogt, U. H. Elizondo, D. Righetti, N. E. Zimmermann, and N. Gruber, 2021: Major restructuring of marine plankton assemblages under global warming. *Nature Communications*, **12,** 5226, 10.1038/s41467-021-25385-x.

Blondeau-Patissier, D., J. F. R. Gower, A. G. Dekker, S. R. Phinn, and V. E. Brando, 2014: A review of ocean color remote sensing methods and statistical techniques for the detection, mapping and analysis of phytoplankton blooms in coastal and open oceans. *Progress in Oceanography*, **123,** 123-144, https://doi.org/10.1016/j.pocean.2013.12.008.

Cole, H., S. Henson, A. Martin, and A. Yool, 2012: Mind the gap: The impact of missing data on the calculation of phytoplankton phenology metrics. *Journal of Geophysical Research: Oceans*, **117**, 10.1029/2012JC008249.

Ghahramani, Z., and M. Jordan, 1993: Supervised learning from incomplete data via an EM approach. *Advances in neural information processing systems*, **6**.

Gobler, C. J., O. M. Doherty, T. K. Hattenrath-Lehmann, A. W. Griffith, Y. Kang, and R. W. Litaker, 2017: Ocean warming since 1982 has expanded the niche of toxic algal blooms in the North Atlantic and North Pacific oceans. *Proceedings of the National Academy of Sciences*, **114,** 4975-4980, 10.1073/pnas.1619575114.

Hilborn, A., and M. Costa, 2018: Applications of DINEOF to Satellite-Derived Chlorophyll-a from a Productive Coastal Region. *Remote Sensing*.

Huntington, H. P., and Coauthors, 2020: Evidence suggests potential transformation of the Pacific Arctic ecosystem is underway. *Nature Climate Change*, 10.1038/s41558-020-0695-2.

Kahru, M., V. Brotas, M. Manzano-Sarabia, and B. G. Mitchell, 2011: Are phytoplankton blooms occurring earlier in the Arctic? *Global Change Biology*, **17,** 1733-1739, 10.1111/j.1365-2486.2010.02312.x.

Keerthi, M. G., C. J. Prend, O. Aumont, and M. Lévy, 2022: Annual variations in phytoplankton biomass driven by small-scale physical processes. *Nature Geoscience*, **15,** 1027-1033, 10.1038/s41561-022-01057-3.

Kurucz, M., A. A. Benczúr, and K. Csalogány, 2007: Methods for large scale SVD with missing values. *Proceedings of KDD cup and workshop*, Citeseer, 31-38.

Lewis, K. M., G. L. van Dijken, and K. R. Arrigo, 2020: Changes in phytoplankton concentration now drive increased Arctic Ocean primary production. *Science*, **369,** 198, 10.1126/science.aay8380.

Liu, X., and M. Wang, 2018: Gap Filling of Missing Data for VIIRS Global Ocean Color Products Using the DINEOF Method. *IEEE Transactions on Geoscience and Remote Sensing*, **56,** 4464-4476, 10.1109/TGRS.2018.2820423.

——, 2019: Filling the Gaps of Missing Data in the Merged VIIRS SNPP/NOAA-20 Ocean Color Product Using the DINEOF Method, **11,** 178.

Mahadevan, A., 2005: Spatial Heterogeneity and Its Relation to Processes in the Upper Ocean. *Ecosystem Function in Heterogeneous Landscapes*, G. M. Lovett, M. G. Turner, C. G. Jones, and K. C. Weathers, Eds., Springer New York, 165-182.

Marchese, C., B. P. V. Hunt, F. Giannini, M. Ehrler, and M. Costa, 2022: Bioregionalization of the coastal and open oceans of British Columbia and Southeast Alaska based on Sentinel-3A satellite-derived phytoplankton seasonality. *Frontiers in Marine Science*, **9**.

Maritorena, S., O. H. F. d'Andon, A. Mangin, and D. A. Siegel, 2010: Merged satellite ocean color data products using a bio-optical model: Characteristics, benefits and issues. *Remote Sensing of Environment*, **114,** 1791-1804, https://doi.org/10.1016/j.rse.2010.04.002.

Sathyendranath, S., and Coauthors, 2019: An Ocean-Colour Time Series for Use in Climate Studies: The Experience of the Ocean-Colour Climate Change Initiative (OC-CCI). *Sensors*, **19,** 4285.

Sheng, Z., W. Weihong, J. Ford, F. Makedon, and J. Pearlman, 2005: Using singular value decomposition approximation for collaborative filtering. *Seventh IEEE International Conference on E-Commerce Technology (CEC'05)*, 257-264.

Smith, K. E., and Coauthors, 2021: Socioeconomic impacts of marine heatwaves: Global issues and opportunities. *Science*, **374,** eabj3593, doi:10.1126/science.abj3593.

Yang, Z., X. Xia, F.-Y. Teo, S.-P. Lim, and D. Yuan, 2023: An Improved DINEOF Algorithm Based on Optimized Validation Points Selection Method. *Water*, **15,** 392.

Zhao, H., 2023: Satellite Perspective on Phytoplankton Bloom Phenology and Linkages With Changing Environments in the Northern High-Latitude Oceans. Ph.D., Indiana State University, 178 pp.

Zhao, H., A. Matsuoka, M. Manizza, and A. Winter, 2022: Recent Changes of Phytoplankton Bloom Phenology in the Northern High-Latitude Oceans (2003–2020). *Journal of Geophysical Research: Oceans*, **127,** e2021JC018346, https://doi.org/10.1029/2021JC018346.